Electronic supplementary material for "Development of an isolation procedure and MC-ICP-MS measurement protocol for the study of stable isotope ratio variations of nickel"

Stepan M. Chernonozhkin, Steven Goderis, Lara Lobo, Philippe Claeys and Frank Vanhaecke

Appendix 1: evaluation of the instrumental mass-discrimination correction model

At the level of natural variation studied, Ni isotope ratio measurements can even be sensitive to the mass bias correction model applied. When the mathematical model assumed for the correction does not fully correspond to the nature of the underlying processes of instrumental mass discrimination and natural isotope fractionation (kinetic/equilibrium), this can result in small under/overcorrections. To examine these undesired artifacts, the application of the flexible generalized power law (GPL) was evaluated. This law is characterized by a variable discrimination exponent *n*.[1] With the application of different values for *n*, the law can take on a mathematical form for equilibrium, kinetic or power law fractionation, or show a mixed character.

$$({}^{x}Ni/{}^{58}Ni)_{corr} = ({}^{x}Ni/{}^{58}Ni)_{meas} \cdot f_{GPL}^{(m_{x}^{n} - m_{58}^{n})} \qquad \text{(A1)}$$

In this equation, $({}^{x}Ni/{}^{58}Ni)_{meas}$ is the measured isotope ratio, m_x and m_{58} are the masses of the Ni isotopes considered, and f_{GPL} represents a fractionation coefficient. The same equation can be written for the isotope ratio of the internal standard. Optimum model discrimination exponents *n* for the GPL can be found for each target element isotope ratio following the method described by Baxter et al.[1,2] Calculation of the optimum discrimination exponent *n* for different isotope ratios of a target element results

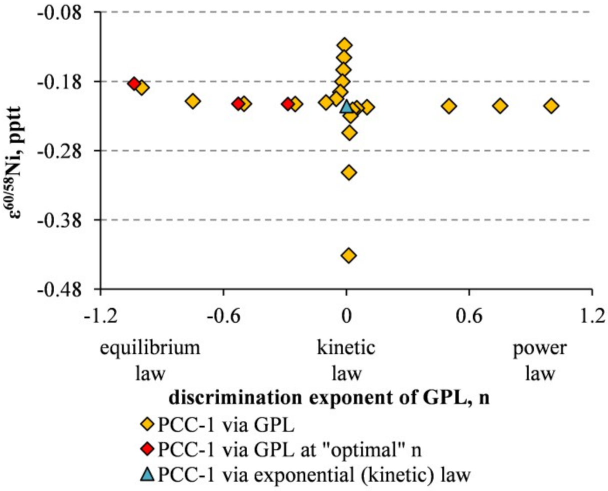

Fig. A1 The results of application of the GPL for the geological reference material peridotite PCC-1 for a varying discrimination exponent *n*. The correction is made using the $^{62/58}$Ni ratio as internal reference. Red diamonds represent the discrimination exponent results with n optimized for three isotope ratios of Ni (see text).

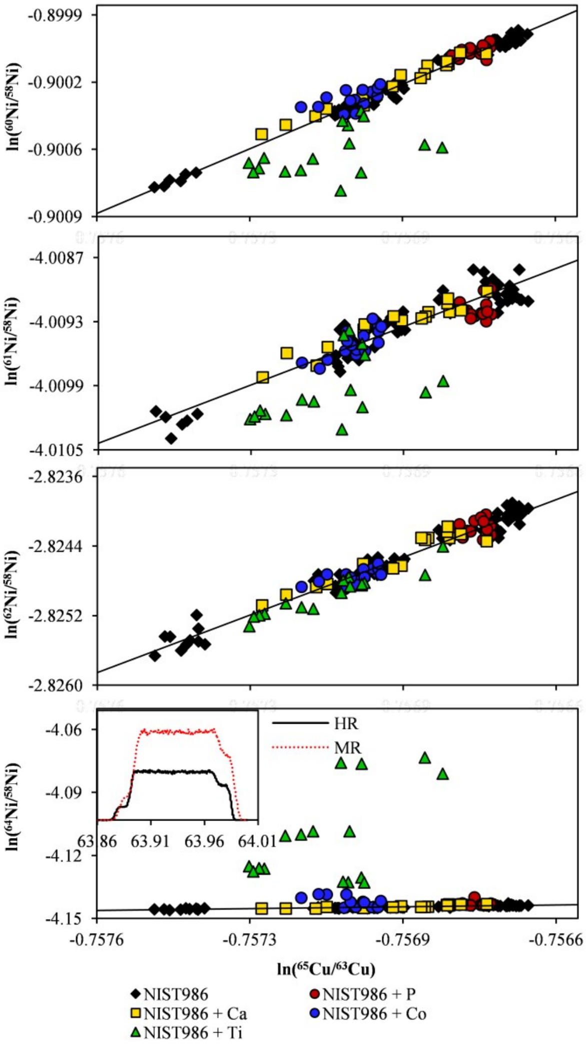

Fig. A2 The effect of particular elements admixed to NIST SRM 986 in relative abundances ranging between 0.1 and 1 on the determined Ni isotope ratios. The ^{64}Ni spectral peak profile shows 1 µg g^{-1} Ni doped with 10 µg g^{-1} Ti at medium and high resolution modes.

Table A1 The list of spectral interferences potentially affecting the measurement of Ni isotopes. Resolution is calculated as $m_{Ni}/\Delta m$, were Δm is calculated based on nuclide masses, taken from Audi *et al.*[3] The quotation of resolving power used for pseudo high resolution mode of MC-ICP-MS exceeds that calculated based on atomic masses by about of a factor of two.[4]

	^{58}Ni (68.3%)		^{60}Ni (26.1%)		^{61}Ni (1.13%)		^{62}Ni (3.59%)		^{64}Ni (0.91%)	
	Interference	$m/\Delta m$	Interference	$m/\Delta m$	Interference	$m/\Delta m$	Interference	$m/\Delta m$	Interference	$m/\Delta m$
Isobars	^{58}Fe (0.28%)	28 060							^{64}Zn (48.6%)	54 314
Hydride ions	$^{57}\text{Fe}^{1}\text{H}^{+}$	7 364	$^{59}\text{Co}^{1}\text{H}^{+}$	5 856	$^{60}\text{Ni}^{1}\text{H}^{+}$	8 065	$^{61}\text{Ni}^{1}\text{H}^{+}$	5 878	$^{63}\text{Cu}^{1}\text{H}^{+}$	6 761
Polyatomic ions	$^{42}\text{Ca}^{16}\text{O}^{+}$	3 189	$^{44}\text{Ca}^{16}\text{O}^{+}$	3 056	$^{45}\text{Sc}^{16}\text{O}^{+}$	3 082	$^{46}\text{Ca}^{16}\text{O}^{+}$	3 056	$^{48}\text{Ti}^{16}\text{O}^{+}$	4 292
	$^{41}\text{K}^{17}\text{O}^{+}$	2 264	$^{43}\text{Ca}^{17}\text{O}^{+}$	2 210	$^{44}\text{Ca}^{17}\text{O}^{+}$	2 586	$^{46}\text{Ti}^{16}\text{O}^{+}$	3 225	$^{48}\text{Ca}^{16}\text{O}^{+}$	3 281
	$^{40}\text{K}^{18}\text{O}^{+}$	2 085	$^{42}\text{Ca}^{18}\text{O}^{+}$	2 220	$^{43}\text{Ca}^{18}\text{O}^{+}$	2 267	$^{45}\text{Sc}^{17}\text{O}^{+}$	2 320	$^{46}\text{Ti}^{18}\text{O}^{+}$	2 683
	$^{40}\text{Ca}^{18}\text{O}^{+}$	2 196	$^{46}\text{Ca}^{14}\text{N}^{+}$	2 307	$^{47}\text{Ti}^{14}\text{N}^{+}$	2 562	$^{44}\text{Ca}^{18}\text{O}^{+}$	2 355	$^{46}\text{Ca}^{18}\text{O}^{+}$	2 569
	$^{44}\text{Ca}^{14}\text{N}^{+}$	2 499	$^{46}\text{Ti}^{14}\text{N}^{+}$	2 405	$^{46}\text{Ti}^{15}\text{N}^{+}$	2 810	$^{48}\text{Ca}^{14}\text{N}^{+}$	2 272	$^{47}\text{Ti}^{17}\text{O}^{+}$	2 788
	$^{43}\text{Ca}^{15}\text{N}^{+}$	2 465	$^{45}\text{Sc}^{15}\text{N}^{+}$	2 375	$^{38}\text{Ar}^{23}\text{Na}^{+}$	2 841	$^{48}\text{Ti}^{14}\text{N}^{+}$	2 731	$^{50}\text{Ti}^{14}\text{N}^{+}$	3 213
	$^{27}\text{Al}^{31}\text{P}^{+}$	2 906	$^{36}\text{Ar}^{24}\text{Mg}^{+}$	2 749	$^{36}\text{Ar}^{25}\text{Mg}^{+}$	2 729	$^{47}\text{Ti}^{15}\text{N}^{+}$	2 632	$^{49}\text{Ti}^{15}\text{N}^{+}$	3 194
	$^{26}\text{Mg}^{32}\text{S}^{+}$	3 002	$^{29}\text{Si}^{31}\text{P}^{+}$	3 078	$^{30}\text{Si}^{31}\text{P}^{+}$	3 698	$^{38}\text{Ar}^{24}\text{Mg}^{+}$	3 187	$^{50}\text{V}^{14}\text{N}^{+}$	2 871
	$^{25}\text{Mg}^{33}\text{S}^{+}$	2 642	$^{28}\text{Si}^{32}\text{S}^{+}$	3 291	$^{29}\text{Si}^{32}\text{S}^{+}$	3 480	$^{36}\text{Ar}^{26}\text{Mg}^{+}$	2 842	$^{50}\text{Cr}^{14}\text{N}^{+}$	3 022
	$^{24}\text{Mg}^{34}\text{S}^{+}$	3 302	$^{27}\text{Al}^{33}\text{S}^{+}$	2 698	$^{28}\text{Si}^{33}\text{S}^{+}$	3 516	$^{27}\text{Al}^{35}\text{Cl}^{+}$	2 809	$^{40}\text{Ar}^{24}\text{Mg}^{+}$	3 285
			$^{26}\text{Mg}^{34}\text{S}^{+}$	3 046	$^{27}\text{Al}^{34}\text{S}^{+}$	3 321	$^{31}\text{P}_{2}^{+}$	3 229	$^{38}\text{Ar}^{26}\text{Mg}^{+}$	3 683
							$^{30}\text{Si}^{32}\text{S}^{+}$	3 540	$^{36}\text{Ar}^{28}\text{Si}^{+}$	3 873
							$^{29}\text{Si}^{33}\text{S}^{+}$	3 158	$^{27}\text{Al}^{37}\text{Cl}^{+}$	3 282
							$^{28}\text{Si}^{34}\text{S}^{+}$	3 765	$^{30}\text{Si}^{34}\text{S}^{+}$	4 673
									$^{31}\text{P}^{33}\text{S}^{+}$	3 705
									$^{32}\text{S}_{2}^{+}$	3 952
									$^{32}\text{S}^{16}\text{O}_{2}^{+}$	1 884
Doubly charged ions	$^{116}\text{Cd}^{2+}$	3 405	$^{120}\text{Sn}^{2+}$	2 951	$^{122}\text{Sn}^{2+}$	2 949	$^{124}\text{Te}^{2+}$	2 685	$^{124}\text{Te}^{2+}$	2 635
	$^{116}\text{Sn}^{2+}$	3 735	$^{120}\text{Te}^{2+}$	2 824	$^{122}\text{Te}^{2+}$	2 977				
Gas-based interferences	$^{40}\text{Ar}^{18}\text{O}^{+}$	2 214	$^{40}\text{Ar}^{20}\text{Ne}^{+}$	2 493	$^{40}\text{Ar}^{21}\text{Ne}^{+}$	2 420	$^{40}\text{Ar}^{22}\text{Ne}^{+}$	2 436	$^{124}\text{Xe}^{2+}$	2 686
	$^{36}\text{Ar}^{22}\text{Ne}^{+}$	2 459	$^{38}\text{Ar}^{22}\text{Ne}^{+}$	2 569			$^{124}\text{Xe}^{2+}$	2 517		
	$^{38}\text{Ar}^{20}\text{Ne}^{+}$	2 925								

in dissimilar *n* (and different corresponding isotope fractionation models) for different isotope ratios.

To correct for the time-dependent variation of instrumental mass discrimination, fractionation coefficients f_{GPL} were calculated for isotope ratios of the target element and the internal standard of all bracketing standards measured in a daily sequence. Fractionation coefficients for the target element and the internal standard were plotted versus each other and a regression line was fitted through the data using the least squares method and the intersection (*a*) and slope (*b*) of the line were calculated. In comparison to the mathematically more correct "York regression"[5], the least square method was found to yield similar Ni isotope ratio results within the associated uncertainty. The calculated linear regression parameters were applied to the measured ratios of the internal standard and used to produce $(^{x}Ni/^{58}Ni)_{corr}$. Finally, sample-standard bracketing was applied to correct for minor drift of instrumental parameters.

The results of the application of the GPL-based model for the geological peridotite reference material PCC-1 with varying discrimination exponent between -1 to +1 are shown in figure A1. This diagram allows a direct comparison of results for a spectrum of different models used for mass bias correction. Varying the optimal discrimination exponent *n* generally results in small overall differences in the final isotope ratio. The optimal discrimination exponents (red diamonds in figure A1) describe the nature of the actual processes underlying natural isotope fractionation of Ni, as mixed between equilibrium (n = -1) and kinetic (n→0). This can be a result of (a) the mixing of different Ni sources; (b) the involvement of multiple natural processes of different nature that fractionate Ni isotopes; (c) the association with kinetic processes that fractionate Ni isotopes when Ni is bound to another element involved.

Because differences between isotope ratios calculated via the GPL with optimized n and kinetic law (n→0) are less than 3 ppm and not resolvable using MC-ICP-MS (see figure A1), the exponential (kinetic) law[6] was found suitable for the correction of mass bias, with the version revised by Baxter found most successful.[7]

Appendix 2: spectral interferences

The medium resolution mode ($m/\Delta m = 7400$) of the Thermo Neptune was used to resolve interfering ion species originating from noble gas atoms in the ICP (ArO^{+}, $ArNe^{+}$, Xe^{2+}). It needs to be stressed that the quotation of resolving power used for the pseudo-high resolution of the MC-ICP-MS unit exceeds that calculated according to the 10 % valley definition by about a factor of two.[4] As such, pairs of ions with $m/\Delta m$ ratios higher than 4500 (were m and Δm denotes ion mass and mass difference respectively, *e.g.* hydrides) cannot be resolved even with the high resolution mode of the instrument. Table A1 lists spectral interferences that can potentially affect the Ni isotope ratios. At

Table A2 Element-to-Ni mass ratios after the complete Ni isolation procedure

		Iron and steel reference materials	Geological reference materials
Isobars	Fe	10^{-6} – 10^{-4}	10^{-4} – 10^{-3}
	Zn	10^{-6} – 10^{-4}	10^{-5} – 10^{-4}
Hydride-forming elements	Co	10^{-5}	10^{-5}
	Cu	10^{-7} – 10^{-5}	10^{-6} – 10^{-5}
Elements forming polyatomic ions	Na	10^{-5} – 10^{-3}	10^{-5} – 10^{-3}
	Mg	10^{-5} – 10^{-3}	10^{-4} – 10^{-3}
	Al	10^{-5} – 10^{-3}	10^{-6} – 10^{-4}
	K	10^{-5} – 10^{-3}	10^{-5} – 10^{-4}
	Ca	10^{-5} – 10^{-3}	10^{-4} – 10^{-3}
	Sc	10^{-8} – 10^{-6}	10^{-5}
	V	10^{-5} – 10^{-3}	10^{-5} – 10^{-3}
	Ti	10^{-5} – 10^{-3}	10^{-6} – 10^{-2}
	Cr	10^{-4} – 10^{-1}	10^{-6} – 10^{-1}
	Mn	10^{-6} – 10^{-4}	10^{-4}
Elements forming doubly charged ions	Cd	10^{-9} – 10^{-6}	10^{-8}
	Sn	10^{-8} – 10^{-6}	10^{-7}
Ni recovery		81 – 87 %	82 – 106 %

the medium resolution mode, minor hydride contributions must be removed by sample-standard bracketing, since the samples and standards should be affected equally. Gas-based interferences cannot be reduced by ion exchange chromatography, but can be corrected for by application of medium instrument resolution mode and sample-standard bracketing. Because of differences in resolving power notations and obscurity of real formation rates of potentially interfering species, the effect of potentially interfering elements listed in Table A1 needs to be evaluated. For this purpose, the NIST SRM 986 Ni isotopic standard was doped with single-element solutions in relative abundances ranging between 0.1 and 1 and measured using the instrument settings described.

Some of the results are presented in figure A2 in the form of linearized three-isotope plots. In the concentration range studied, only Ti appears to affect the ^{60}Ni/^{58}Ni, ^{61}Ni/^{58}Ni and ^{64}Ni/^{58}Ni ratios. The most significant effects are observed for ratios involving the least abundant ^{64}Ni isotope. The theoretical mass resolution, calculated based on atomic masses, needed to resolve Ti species from ^{64}Ni is about of 3200. This mass resolution is not achieved in medium resolution, but can be achieved in the high mass-resolution mode of the instrument (see figure A2). The peak profiles of a 1 µg g^{-1} Ni solution doped with 10 µg g^{-1} Ti in medium and high mass-resolution modes are shown in figure A2.

Appendix 3: evaluation of the Ni isolation procedure

Table A2 presents the element to Ni mass ratios in steel and geological reference materials after the complete Ni isolation procedure.

List of references

1 F. Wombacher and M. Rehkamper, *J. Anal. At. Spectrom.*, 2003, **18**, 1371–1375.

2 D. C. Baxter, I. Rodushkin and E. Engström, *J. Anal. At. Spectrom.*, 2012, **27**, 1355–1381.

3 G. Audi, A. H. Wapstra and C. Thibault, *Nucl. Phys. A*, 2003, **729**, 337–676.

4 F. Vanhaecke and L. Moens, *Anal. Bioanal. Chem.*, 2004, **378**, 232–240.

5 D. York, *Can. J. Phys.*, 1966, **44**, 1079–1086.

6 W. A. Russell, D. A. Papanastassiou and T. A. Tombrello, *Geochim. Cosmochim. Acta*, 1978, **42**, 1075–1090.

7 D. C. Baxter, I. Rodushkin, E. Engström and D. Malinovsky, *J. Anal. At. Spectrom.*, 2006, **21**, 427–430.